


ORIGINAL ARTICLE

Open Access



Modeling and Parameter Sensitivity Analysis of Valve-Controlled Helical Hydraulic Rotary Actuator System

Kun Zhang¹, Junhui Zhang^{1*} , Minyao Gan², Huaizhi Zong¹, Ximeng Wang¹, Hsinpu Huang¹, Qi Su¹ and Bing Xu¹

Abstract

As a type of hydraulic rotary actuator, a helical hydraulic rotary actuator exhibits a large angle, high torque, and compact structure; hence, it has been widely used in various fields. However, its core technology is proprietary to several companies and thus has not been disclosed. Furthermore, the relevant reports are primarily limited to the component level. The dynamic characteristics of the output when a helical rotary actuator is applied to a closed-loop system are investigated from the perspective of driving system design. Two main aspects are considered: one is to establish a reliable mathematical model and the other is to consider the effect of system parameter perturbation on the output. In this study, a detailed mechanical analysis of a helical rotary hydraulic cylinder is first performed, factors such as friction and load are considered, and an accurate dynamic model of the actuator is established. Subsequently, considering the nonlinear characteristics of pressure flow and the dynamic characteristics of the valve, a dynamic model of a valve-controlled helical rotary actuator angle closed-loop system is described based on sixth-order nonlinear state equations, which has never been reported previously. After deriving the system model, a sensitivity analysis of 23 main parameters in the model with a perturbation of 10% is performed under nine operating conditions. Finally, the system dynamics model and sensitivity analysis results are verified via a prototype experiment and co-simulation, which demonstrate the reliability of the theoretical results obtained in this study. The results provide an accurate mathematical model and analysis basis for the structural optimization or control compensation of similar systems.

Keywords: Helical hydraulic rotary actuator, Dynamic model, Closed-loop system, Sensitivity analysis, Prototype experiment, Co-simulation

1 Introduction

Helical hydraulic rotary actuators (HHRAs) are hydraulic actuators that convert hydraulic energy into mechanical energy via rotary motion [1]. Compared with conventional rotary hydraulic actuators, such as vane-, rack-, and gear- type ones, helical rotary actuators offer a large rotation angle, high output torque, compact structure, and high volumetric efficiency owing to their unique

double helical pair structure [2, 3]. The rotation angle range of a helical actuator can be designed to exceed 360°. Furthermore, for the same rotation angle range, the helical actuator typically exhibits a small weight and volume, which renders the structure installed with it compact [4]. Furthermore, the helical actuator can achieve a higher actuating pressure than the conventional rotary actuator. It can maintain a high efficiency at 21 MPa, which cannot be realized by other forms of hydraulic rotary actuators [5]. Because of these outstanding characteristics, helical rotary actuators have been widely used in certain applications that require large torques, large rotation angles, and limited installation space, e.g., agricultural, construction,

*Correspondence: benzjh@zju.edu.cn

¹ State Key Laboratory of Fluid Power and Mechatronic Systems, Zhejiang University, Hangzhou 310027, China
Full list of author information is available at the end of the article

and mining machinery [6, 7]. However, only a few companies can manufacture such actuators currently [6–9], and the core technologies for design and manufacturing remain proprietary. Studies regarding HHRAs, in addition to some patents [10–12], focus primarily on the component level, including the structural design, dynamic models, flow field analysis, transmission efficiency, and sealing [13–16].

The performance of a valve-controlled actuator system, as a driving unit, directly affects the control performance of the entire machine [17]. Such systems are typically designed using mathematical models derived from constant-coefficient ordinary differential equations [18]. However, two problems are encountered: First, studies regarding helical rotary actuator driving systems are scarce. Furthermore, the dynamic model of the rotary actuator described in the literature is relatively simple [2, 3] and may not be sufficiently accurate when modeling analysis is required. Therefore, reliable mathematical models for the design and analysis of hydraulic systems are insufficient. The other problem is that the parameters in the model are typically regarded as constants [19]; however, these parameters may not be consistent with the parameters in practical applications because the system parameters are time varying [20]. For example, structural wear results in parameter changes, inaccurate valve test parameters, and pressure fluctuations in the hydraulic system. To obtain a valve-controlled actuator system that satisfies the design requirements, the effect of parameter perturbation on the dynamic characteristics of the system is to be investigated; therefore, a sensitivity analysis of the system parameters is required.

Sensitivity analysis can be performed via several methods, which can be classified into sensitivity functions in the time domain, frequency domain, and the performance-index sensitivity, each of which offers its own advantages and application range [21]. Sensitivity analysis theory is widely used in mechanical design, power systems, water conservancy systems, etc. [22–24]. In the application of hydraulic systems, trajectory sensitivity analysis in the time domain is most typically used method and can be used for nonlinear systems with time-varying parameters. Vilenius et al. [20] introduced and applied a sensitivity model suitable for deadband-type nonlinearities in a typical servo system used in the sawmill industry. They simplified the valve-controlled actuator system into a fifth-order model and derived a first-order trajectory sensitivity mathematical expression of the system. Under a single operating condition, the sensitivity of the system parameters was defined when the 10 main parameters changed by 1%. Kim et al. [25] used a fourth-order

state equation to analyze the nonlinear dynamics of an axial piston pump system and analyzed the sensitivity of the parameters in the model using a first-order sensitivity equation. Pietola et al. [26, 27] investigated the transient-state and steady-state parameter sensitivity of a heavily loaded flexible electro-hydraulic position servo system and then compared three control methods, i.e., P-control, model reference control, and P + PID/ \dot{x} -control. Farahat et al. [21] constructed a fourth-order linear mathematical model of an electro-hydraulic servo position control system. The position control sensitivity of the valve-controlled actuator system to 18 main parameters based on a 1% change is investigated, and four sensitivity indices are presented. Kong et al. [28, 29] established a sixth-order nonlinear model of a valve-controlled actuator system based on position control, and the influence degree and rules of 10% parameter changes with respect to the displacement output response were obtained using the first-order trajectory sensitivity method. Subsequently, they deduced the method of second-order trajectory sensitivity and analyzed its effect on the system displacement step response with parameter variation (10% and 20%) under nine operating conditions. Ba et al. [30–32] proposed a first-order sensitivity matrix method and applied it to the dynamic sensitivity analysis of the valve-controlled actuator system of a legged robot. Huang et al. [33] used the first-order trajectory sensitivity method to determine the dominant parameters of the electro-hydraulic actuator in a legged robot and then estimated them online in real time.

The main difference among the studies above is the degree of simplification of the hydraulic system model. The sensitivity analysis methods are similar and are based on trajectory sensitivity. However, the hydraulic actuators reported in the literature are linear actuators, and a sensitivity analysis of the helical rotary actuator-driven system has not been reported. Compared with linear actuators, helical rotary actuators are more complex in terms of structure, and their model parameters are numerous; therefore, the results of parameter sensitivity analysis for those two types of actuators may be different.

To design and analyze the dynamic characteristics of a valve-controlled helical rotary actuator system, in this study, a relatively accurate dynamic model of an actuator was established. A mechanical analysis of the designed helical rotary actuator was performed, and the friction between different components and load types was considered. Subsequently, considering the nonlinear characteristics of pressure and flow at the valve port and the dynamic characteristics of the servo valve, a sixth-order nonlinear state equation was established to describe

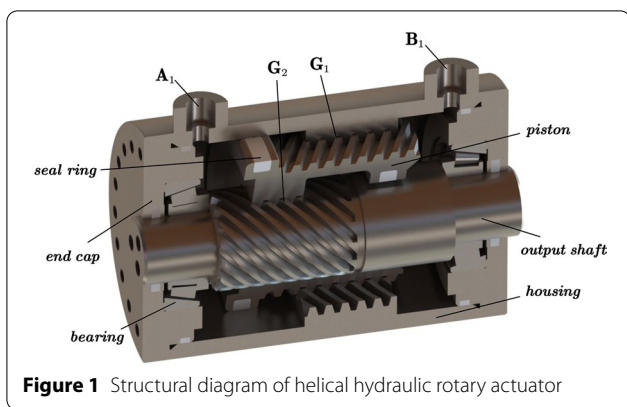


Figure 1 Structural diagram of helical hydraulic rotary actuator

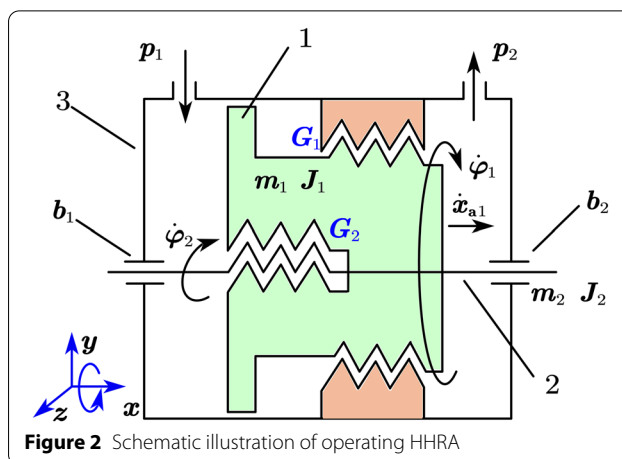


Figure 2 Schematic illustration of operating HHRA

an angular displacement closed-loop hydraulic system. Under different step input and load conditions, the sensitivities of 23 parameters in the closed-loop system model were solved using the first-order trajectory sensitivity analysis method. Finally, the dynamic model and sensitivity analysis results of the system were verified by experiments and co-simulation, respectively, and a sensitivity index was used to explain the sensitivity results comprehensively.

The remainder of this paper is organized as follows: In Section 2, a dynamic model of the helical rotary actuator is deduced, and a mathematical model of the closed-loop system is presented. The parameter sensitivity equation of the system is presented in Section 3. Details regarding the experiment and co-simulation verification are provided in Section 4. Finally, a summary is presented in Section 5.

2 Nonlinear Dynamic Model of System

The angular displacement closed-loop system of a valve-controlled HHRA is the research object of this study. In the following, the dynamic model of the rotary actuator is first established, and then the servo valve and proportional controller are introduced to establish the model of the entire hydraulic system.

2.1 Basic Operating Principle of HHRA

The basic structure of the designed HHRA is shown in Figure 1. It is primarily composed of a housing with an integral ring gear and two moving components: an output shaft and an annular piston sleeve. A_1 and B_1 represent the oil inlet and outlet, respectively. The helical spline teeth on the outside diameter of the piston engage in matching the splines of the housing ring gear (helical pair G_1), and the inside diameter of the piston houses a second set of

splines of the opposite hand, which engages the matching splines of the output shaft (helical pair G_2). The seal ring on the piston segregates the housing into two independent chambers. When hydraulic pressure is applied, the piston actuates axially relative to the housing, similar to a hydraulic linear actuator. Simultaneously, owing to G_1 , the piston rotates and finally exhibits helical motion. When the piston is actuating helically, it drives the output shaft to rotate under the action of G_2 . Therefore, the rotational direction of the output shaft can be controlled by filling the pressure oil into different oil ports (A_1 or B_1).

2.2 Dynamic Model of HHRA

Based on the operating principle described in the previous section, the HHRA is schematically illustrated (as shown in Figure 2). It is composed of a piston (label 1), an output shaft (label 2), housing (label 3), and bearings (labels b_1 and b_2). The housing was fixed, and the axial displacement of the output shaft was limited by the bearings. The relative motion components are primarily G_1 and G_2 , i.e., the helical motion of the piston and the rotation of the output shaft, respectively. To facilitate analysis, it is assumed that the pressure oil is introduced into the left chamber of the actuator, and the right chamber of the actuator returns oil. The motion states of the piston and shaft in this case are shown in Figure 2.

Kinematic analysis should first be performed prior to dynamic modelling. Because the HHRA is a system with one degree-of-freedom, once the displacement or rotation angle of the piston is determined, the motion state of the entire system can be determined. The state variables exhibit the following kinematic relationships:

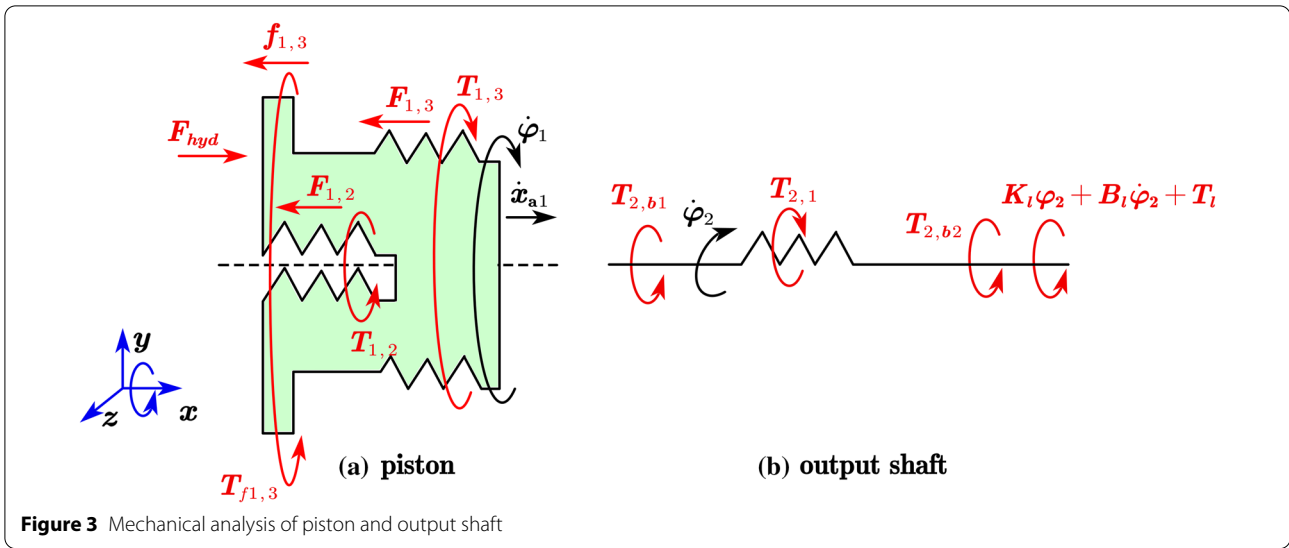


Figure 3 Mechanical analysis of piston and output shaft

$$\varphi_1 = \frac{2\pi x_{a1}}{S_1}, \tag{1}$$

$$\varphi_2^1 = \frac{2\pi x_{a1}}{S_2}, \tag{2}$$

$$\varphi_2 = \varphi_1 + \varphi_2^1 = \frac{2\pi x_{a1}(S_1 + S_2)}{S_1}, \tag{3}$$

where φ_1 is the rotation angle of the piston relative to the housing; φ_2^1 is the angle of the output shaft relative to the piston; φ_2 is the angle of the output shaft relative to the housing; x_{a1} is the axial displacement of the piston; S_1 and S_2 are the leads of G_1 and G_2 , respectively. After obtaining the kinematic relationship, a mechanical analysis of the piston and output shaft was performed, an illustration of which is presented in Figure 3.

The forces and moments exerting on the piston are shown in Figure 3(a). Considering the coordinate system direction in the figure as the positive direction, the dynamic equations of the piston can be expressed as follows:

$$F_{hyd} - f_{1,3} - F_{1,3} - F_{1,2} = m_1 \ddot{x}_{a1}, \tag{4}$$

$$T_{1,3} - T_{1,2} - T_{f1,3} = J_1 \ddot{\varphi}_1, \tag{5}$$

where F_{hyd} is the resultant force generated by the oil pressure in the two chambers of the actuator; m_1 is the mass of the piston; J_1 is the moment of inertia of the piston; $F_{1,3}$ and $F_{1,2}$ are the axial forces generated by G_1 and G_2 respectively; $T_{1,3}$ and $T_{1,2}$ are the torques generated by G_1 and G_2 , respectively; $f_{1,3}$ and $T_{f1,3}$ are the force and torque

caused by friction between the seal ring on the piston and housing, respectively. The moments on the output shaft (as no movement exists in the axial direction of the output shaft, only the moments are presented herein) are shown in Figure 3(b). Considering the load characteristics, the dynamic equation is expressed as follows:

$$T_{2,1} - T_{2,b1} - T_{2,b2} = J_2 \ddot{\varphi}_2 + B_l \dot{\varphi}_2 + K_l \varphi_2 + T_l, \tag{6}$$

where $T_{2,1}$ is the torque generated by G_2 ; $T_{2,1} = T_{1,2}$; $T_{2,b1}$ and $T_{2,b2}$ are the torques generated by the bearing friction; J_2 is the moment of inertia of the output shaft and load; B_l is the load damping coefficient; K_l is the load stiffness coefficient; T_l is the external load torque. Meanwhile, forces $F_{1,3}$, $F_{1,2}$ and torques $T_{1,3}$, $T_{1,2}$ caused by G_1 and G_2 can be obtained via a mechanical analysis of the helical pair, as shown in Figure 4.

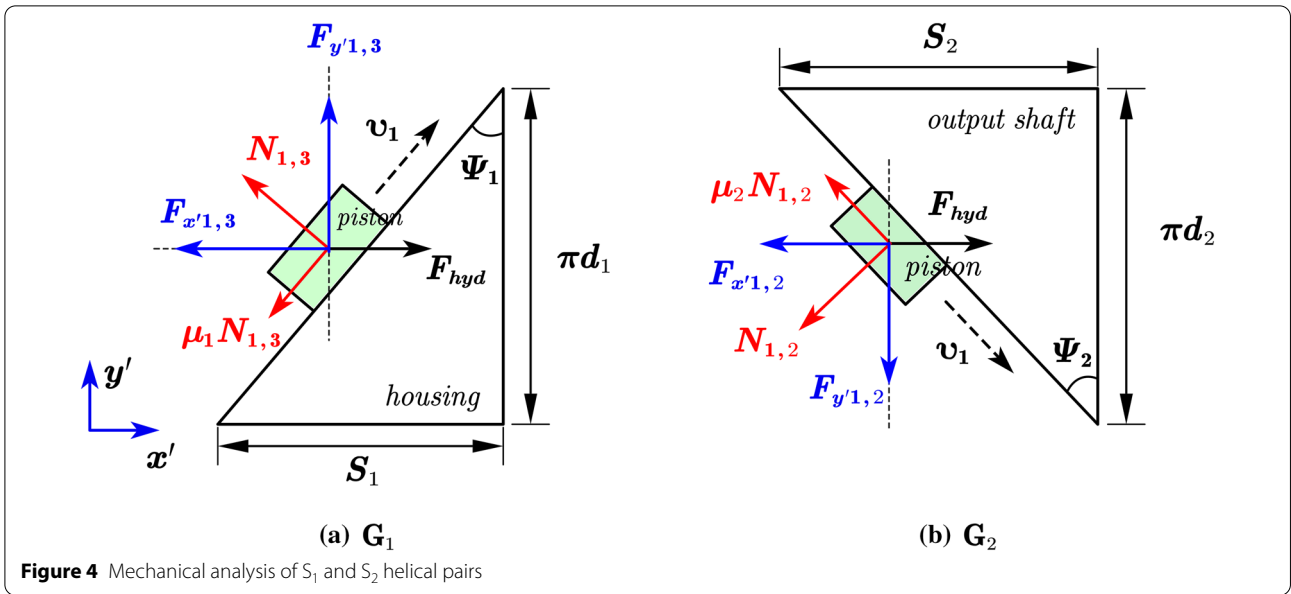
Because the effect of piston gravity on the helical pair depends on the installation position, to simplify the analysis, the output shaft is assumed to be installed horizontally; thus, the effect of gravity is negligible. As shown in Figures 4(a) and (b), $F_{1,3}$, $T_{1,3}$, $F_{1,2}$, and $T_{1,2}$ are calculated as follows:

$$F_{1,3} = F_{x'1,3} = N_{1,3}(\cos \lambda_1 + \mu_1 \sin \Psi_1), \tag{7}$$

$$T_{1,3} = \frac{F_{y'1,3}d_1}{2} = \frac{N_{1,3}(\sin \lambda_1 - \mu_1 \cos \Psi_1)d_1}{2}, \tag{8}$$

$$F_{1,2} = F_{x'1,2} = N_{1,2}(\cos \lambda_2 + \mu_2 \sin \Psi_2), \tag{9}$$

$$T_{1,2} = \frac{F_{y'1,2}d_2}{2} = \frac{N_{1,2}(\sin \lambda_2 - \mu_2 \cos \Psi_2)d_2}{2}, \tag{10}$$



where $N_{1,3}$ and $N_{1,2}$ are the normal forces produced by G_1 and G_2 , respectively; μ_1 and μ_2 are the dynamic friction coefficients of G_1 and G_2 , respectively; Ψ_1 and Ψ_2 are the helix angles of G_1 and G_2 , respectively; d_1 and d_2 are the pitch diameters of G_1 and G_2 , respectively. The resultant force generated by the oil pressure F_{hyd} can be expressed as

$$F_{hyd} = (p_1 - p_2)A_p, \tag{11}$$

where p_1 is the oil pressure in the left chamber of the actuator, p_2 the pressure in the right chamber, and A_p the effective action area of the piston. According to Eqs. (1)–(11), the dynamic equation of the HHRA can be expressed as follows:

$$(p_1 - p_2)A_p = A\ddot{\varphi}_2 + B\dot{\varphi}_2 + C\varphi_2 + D, \tag{12}$$

where $A = Q_1 \cdot \left(\frac{J_1 S_2}{S_1 + S_2} + J_2 \right) + Q_2 \cdot J_2 + \frac{m_1 S_1 S_2}{2\pi(S_1 + S_2)}$,
 $B = (Q_1 + Q_2) \cdot B_l, C = (Q_1 + Q_2) \cdot K_l,$
 $D = Q_1 \cdot (T_{f1,3} + T_{2,b1} + T_{2,b2} + T_l) +$
 $Q_2 \cdot (T_{2,b1} + T_{2,b2} + T_l) + f_{1,3},$
 $Q_1 = \frac{2(\cos \lambda_1 + \mu_1 \sin \Psi_1)}{d_1(\sin \lambda_1 - \mu_1 \cos \Psi_1)}, Q_2 = \frac{2(\cos \lambda_2 + \mu_2 \sin \Psi_2)}{d_2(\sin \lambda_2 - \mu_2 \cos \Psi_2)}.$

2.3 Dynamic Model of Valve-Controlled HHRA System

In this study, an angle closed-loop system is investigated using a servo valve, and a schematic diagram of the valve-controlled actuator system is shown in Figure 5. The flow at the valve port is expressed as follows:

$$q_1 = \begin{cases} K_d x_v \sqrt{p_s - p_1} & \text{for } x_v \geq 0, \\ K_d x_v \sqrt{p_1 - p_0} & \text{for } x_v < 0, \end{cases} \tag{13}$$

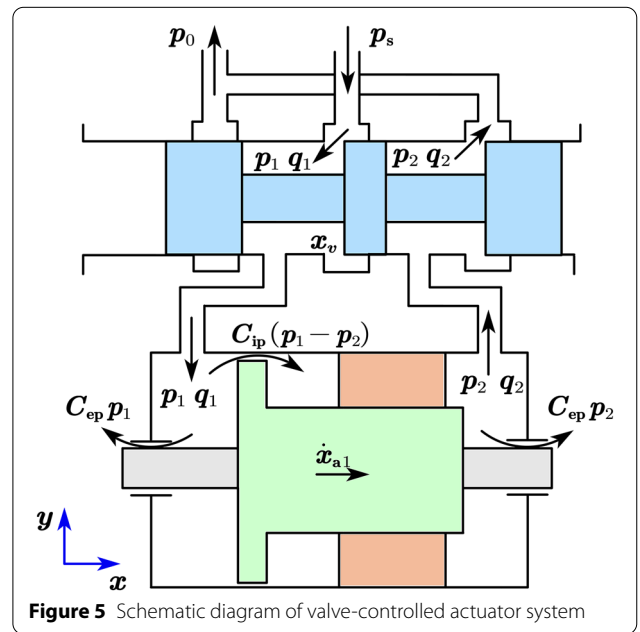


Figure 5 Schematic diagram of valve-controlled actuator system

$$q_2 = \begin{cases} K_d x_v \sqrt{p_2 - p_0} & \text{for } x_v \geq 0, \\ K_d x_v \sqrt{p_s - p_2} & \text{for } x_v < 0, \end{cases} \tag{14}$$

where x_v denotes the valve spool displacement, p_s the supply pressure, p_0 the return oil pressure, and K_d the converted flow coefficient. Considering the effects of oil leakage and compressibility, the flow continuity equations for the HHRA can be written as follows:

$$q_1 = A_p \dot{x}_{a1} + \frac{V_{g1} + A_p L_0 + A_p x_{a1}}{\beta_e} \dot{p}_1 + C_{ip}(p_1 - p_2) + C_{ep} p_1, \tag{15}$$

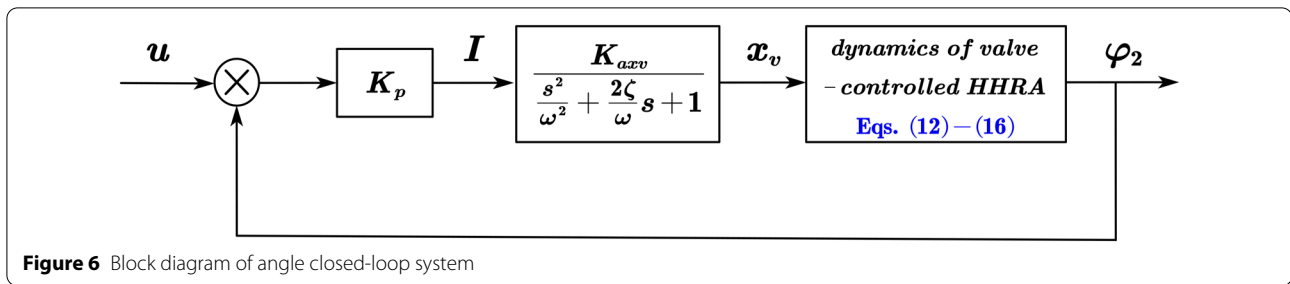


Figure 6 Block diagram of angle closed-loop system

$$q_2 = A_p \dot{x}_{a1} - \frac{V_{g2} + A_p(L - L_0) - A_p x_{a1}}{\beta_e} \dot{p}_2 + C_{ip}(p_1 - p_2) - C_{ep} p_2, \tag{16}$$

where β_e is the effective bulk modulus of the system; V_{g1} and V_{g2} are the volumes of the oil inlet and outlet channels connecting the valve and actuator, respectively; L is the maximum axial stroke of the piston; L_0 is the initial axial position of the piston; C_{ip} is the internal leakage coefficient of the actuator; C_{ep} is the external leakage coefficient.

A second-order differential equation was used to approximate the dynamics of the servo valve, as follows:

$$\ddot{x}_v + 2\zeta\omega\dot{x}_v + \omega^2x_v = K_{axv}\omega^2I, \tag{17}$$

where ζ is the damping ratio of the valve, ω the natural frequency of the valve, K_{axv} the gain of the valve, and I the input signal of the valve. The characteristics of the angle closed-loop control can be expressed as follows:

$$I = K_p(u - \varphi_2), \tag{18}$$

where K_p is the gain of the P controller, and u is the input signal. The block diagram of the valve-controlled HHRA system based on the angular displacement closed-loop control is established using Eqs. (12)–(18), as shown in Figure 6.

The state-space equation is used to describe the sixth-order system, and the state variables are selected as follows:

$$\mathbf{x} = [x_1, x_2, x_3, x_4, x_5, x_6]^T = [\varphi_2, \dot{\varphi}_2, x_v, \dot{x}_v, p_1, p_2]^T,$$

The state equation of the valve-controlled HHRA system is obtained as follows:

$$\begin{bmatrix} \dot{x}_1 \\ \dot{x}_2 \\ \dot{x}_3 \\ \dot{x}_4 \\ \dot{x}_5 \\ \dot{x}_6 \end{bmatrix} = \begin{bmatrix} x_2 \\ -\frac{B}{A}x_2 - \frac{C}{A}x_1 + \frac{A_p}{A}x_5 - \frac{A_p}{A}x_6 - \frac{D}{A} \\ x_4 \\ \omega^2K_pK_{axv}u - \omega^2K_pK_{axv}x_1 - 2\zeta\omega x_4 - \omega^2x_3 \\ \frac{\beta_e}{V_{g1} + \Gamma(\varphi_{20} + x_1)} [K_d x_3 \sqrt{\Delta_1} - (C_{ip} + C_{ep})x_5 + C_{ip}x_6 - \Gamma x_2] \\ \frac{\beta_e}{V_{g2} + \Gamma(\varphi_{2\max} - \varphi_{20} - x_1)} [-K_d x_3 \sqrt{\Delta_2} - (C_{ip} + C_{ep})x_6 + C_{ip}x_5 + \Gamma x_2] \end{bmatrix}, \tag{19}$$

where $\Gamma = \frac{A_p S_1 S_2}{2\pi(S_1 + S_2)}$,
 $\Delta_1 = \frac{[1 + \text{sgn}(x_v)]p_s}{2} + \frac{[-1 + \text{sgn}(x_v)]p_0}{2} - \text{sgn}(x_v)p_1$,
 $\Delta_2 = \frac{[1 - \text{sgn}(x_v)]p_s}{2} + \frac{[-1 - \text{sgn}(x_v)]p_0}{2} + \text{sgn}(x_v)p_2$,
 here, φ_{20} is the initial angle of the output shaft, and $\varphi_{2\max}$ is the maximum angle of the output shaft.

3 Sensitivity Model and Analysis

The actual system parameters exhibit varying degrees of perturbation. When the system is sensitive to certain parameters, this perturbation will render the actual output significantly different from that of the mathematical model, which may result in deviation from the design requirements. Analyzing the parameter sensitivity allows us identify these key parameters such that the appropriate response measures can be implemented to reduce the parameter sensitivity or the parameters can be optimized. In this study, the first-order sensitivity method was selected to analyze the effect of 10% perturbation from the nominal parameter value on the rotation angle of the output shaft φ_2 . This method is sufficiently accurate and allows an easier calculation than the high-order sensitivity method [29].

3.1 First-Order Trajectory Sensitivity Equation of System

Based on Eq. (19), many different types of parameters exist in the system dynamics model, including the structural parameters of the HHRA, operating parameters, parameters of the servo valve, and control parameters. The fluctuations of the different parameters are of different timescales. In this study, 23 main parameters in the system model were selected, which encompassed all types of parameters, as follows:

$$\alpha = [J_1, J_2, S_1, S_2, \Psi_1, \Psi_2, \mu_1, \mu_2, d_1, d_2, m_1, A_p, \varphi_{2\max}, \varphi_{20}, \beta_e, C_{ip}, K_d, p_s, p_0, \omega, \zeta, K_{axv}, K_p].$$

The actual structural parameters of the HHRA (α_1 – α_{13}) are associated with the manufacturing errors and wear degree of the corresponding parts. Therefore, they will not change in the short term but may change after the system operates for a long time owing to wear. Owing to changes in the gas content, oil temperature, and load conditions, the operating parameters (α_{14} – α_{19}) are not constant but in a state of rapid dynamic fluctuation. Because the nonlinear high-order dynamic characteristics of the servo valve are simplified into a second-order differential equation, the real dynamic characteristics cannot be fully described. Therefore, the parameters of the servo valve (α_{20} – α_{22}) are not fixed and are affected by the input signal and operating parameters. The control parameter α_{23} must be dynamically adjusted with the change in system conditions to maintain the robustness of the system performance. Because the parameters above may exhibit different degrees of perturbation, the effects of the variations in the parameters above on the output characteristics of the system must be analyzed to improve the performance of the system.

The dynamics and sensitivity equations of the closed-loop system can be expressed as follows [20]:

$$\begin{cases} \dot{\mathbf{x}} = f(\mathbf{x}, \mathbf{u}, \boldsymbol{\alpha}, t), & \text{(a)} \\ \dot{\boldsymbol{\lambda}}^i = \left(\frac{\partial f}{\partial \mathbf{x}}\right)_n \boldsymbol{\lambda}^i + \left(\frac{\partial f}{\partial \boldsymbol{\alpha}_i}\right)_n, & \text{(b)} \end{cases} \quad (20)$$

where $\boldsymbol{\lambda}^i = \left(\frac{\partial \mathbf{x}}{\partial \boldsymbol{\alpha}_i}\right)_n$ is the sensitivity function of parameter $\boldsymbol{\alpha}_i$, $i = 1, \dots, 23$.

The vector is written as follows:

$$\mathbf{x} = [x_1 \ x_2 \ x_3 \ x_4 \ x_5 \ x_6]^T, \quad \mathbf{u} = [u \ T_l]^T.$$

Assuming that the initial state is zero, the initial conditions for Eq. (20) are

$$\begin{cases} \mathbf{x}_0 = \mathbf{0}, \\ \boldsymbol{\lambda}_0^i = \left(\frac{\partial \mathbf{x}_0}{\partial \boldsymbol{\alpha}_i}\right)_n = \mathbf{0}. \end{cases} \quad (21)$$

Once the sensitivity functions are obtained, the variation of the state caused by parameter perturbation can be determined using the following equation (based on the Taylor theorem and disregarding higher-order terms):

$$\delta \mathbf{x} = \left(\frac{\partial \mathbf{x}}{\partial \boldsymbol{\alpha}}\right)_n \delta \boldsymbol{\alpha}. \quad (22)$$

3.2 Solutions of Sensitivity Function

To solve Eq. (20), the values of the nominal parameters are determined, as shown in Table 1. The structural parameters of HHRA are consistent with those in the

Table 1 Nominal value of parameters

Parameter	Description	Value	Units
$\alpha_{1n} = J_1$	Moment of inertia of the piston	8.368×10^{-4}	kg·m ²
$\alpha_{2n} = J_2$	Moment of inertia of the output shaft	1.057×10^{-4}	kg·m ²
$\alpha_{3n} = S_1$	Lead of G_1	0.12	m
$\alpha_{4n} = S_2$	Lead of G_2	0.09	m
$\alpha_{5n} = \psi_1$	Helix angle of G_1	29.324	°
$\alpha_{6n} = \psi_2$	Helix angle of G_2	40.962	°
$\alpha_{7n} = \mu_1$	Dynamic friction coefficients of G_1	0.005	–
$\alpha_{8n} = \mu_2$	Dynamic friction coefficients of G_2	0.005	–
$\alpha_{9n} = d_1$	Pitch diameter of G_1	0.068	m
$\alpha_{10n} = d_2$	Pitch diameter of G_2	0.033	m
$\alpha_{11n} = m_1$	Mass of piston	0.969	kg
$\alpha_{12n} = A_p$	Effective action area of piston	3.951×10^{-3}	m ²
$\alpha_{13n} = \varphi_{2\max}$	Maximum angle of output shaft	178.5	°
$\alpha_{14n} = \varphi_{20}$	Initial angle of output shaft	14	°
$\alpha_{15n} = \beta_e$	Effective bulk modulus of system	6.85×10^8	N/m ²
$\alpha_{16n} = C_{ip}$	Internal leakage coefficient of actuator	3×10^{-14}	m ³ /(s·Pa)
$\alpha_{17n} = K_d$	Converted flow coefficient	4.95×10^{-4}	m ² /(s·√Pa)
$\alpha_{18n} = p_s$	Supply pressure	18×10^6	Pa
$\alpha_{19n} = p_0$	Return oil pressure	0.1×10^6	Pa
$\alpha_{20n} = \omega$	Natural frequency of valve	134	rad/s
$\alpha_{21n} = \zeta$	Damping ratio of valve	1.1	–
$\alpha_{22n} = K_{axv}$	Gain of valve	0.433	m/A
$\alpha_{23n} = K_p$	Gain of P controller	0.001	–

three-dimensional (3D) model. The parameters of the servo valve were obtained from the dynamic characteristic curve in the stylebook. The values of the operating parameters, control parameters, and other parameters that are difficult to determine were selected based on application requirements and engineering experience.

Second, Eq. (20a) was established and solved using MATLAB SIMULINK to obtain the state \mathbf{x} at every moment. The step input is generally believed to be the most severe operating state of the system; therefore, the step signal was used as the input signal to evaluate the dynamic performance of the system. The dynamic response characteristics of the system were different under different values of angular displacement and load conditions. Therefore, to encompass various operating conditions, step signals of 45°, 90°, and 135° were used as inputs, and the external load torques of “no load,” 100 N·m, and 200 N·m were used, respectively. The step

Table 2 Working conditions

Condition	Amplitude (°)	Load torque (N·m)
1	45	0
2	90	0
3	135	0
4	45	100
5	90	100
6	135	100
7	45	200
8	90	200
9	135	200

response of the angular displacement closed-loop system was solved under nine operating conditions, all of which are listed in Table 2.

After solving the state equations, the state value of each moment within the calculation duration was obtained. The results were converted into the coefficient matrix and free matrix of Eq. (20b). Subsequently, using MATLAB, the fourth-order Runge–Kutta method was applied to solve the first-order trajectory sensitivity equations. Finally, the sensitivity functions of the angular displacement step response to 23 parameters were obtained under nine different conditions. Because the sensitivity function curves of some parameters are of different orders of magnitude under no-load and load conditions, for brevity, only the sensitivity function solutions of different step signals under no-load conditions are presented herein, as shown in Figure 7.

The curve in Figure 7 shows the dynamic sensitivity of each parameter to the rotation angle of the output shaft within 0.3 s. Owing to the different ranges of nominal values, the sensitivity functions of different parameters exhibit different orders of magnitude, rendering it difficult to intuitively compare the sensitivity of various parameters from the figure. Eq. (22) was used to clarify the results, and the variation in the angle was obtained based on the sensitivity function of different parameters to uniformly characterize the effect of each parameter. The effect of 10% fluctuation of each parameter on x_1 under the nine conditions is illustrated in Figure 8.

As shown in Figure 8, under the no-load conditions, the parameters that are the most sensitive to the rotation angle are α_{12} , α_{17} , α_{22} , and α_{23} , in which the curves corresponding to α_{17} , α_{22} , and α_{23} are exactly the same. This is followed by parameters α_3 , α_4 , α_{18} , α_{20} , and α_{21} , whereas the other parameters barely affect the rotation angle. However, as the load increases, parameters α_5 , α_6 , α_9 , and α_{10} becomes more sensitive gradually,

and their effect on the rotation angle is not negligible. Meanwhile, some parameters fluctuated during the initial stage. The amplitude of the fluctuation increases with the load but decays rapidly. Only qualitative results can be obtained, and a more detailed quantitative analysis of the sensitivity of each parameter is presented in Section 4.3.

4 Experiment and Co-Simulation Verification

A valve-controlled actuator test platform was constructed to verify the accuracy of the system dynamics model in this study. Subsequently, the theoretical calculation results of parameter sensitivity were verified via co-simulation. To validate the theoretical sensitivity results, the effect of slight parameter changes on the system must be analyzed. However, slight changes in some parameters are difficult to measure accurately in the prototype experiment. For example, pressure pulsation occurs in the system pressure, and the pressure sensor may be affected by noise; therefore, accurately increasing or decreasing the pressure by approximately 10% is challenging. Moreover, the structural parameters or some operating parameters cannot be changed in the prototype experiment. Hence, the results of the sensitivity analysis were verified via co-simulation using MATLAB and Adams.

4.1 Dynamic Model Verification of Valve-Controlled HHRA System

The valve-controlled HHRA test platform and a schematic diagram of the system are shown in Figure 9. The closed-loop system primarily includes a rotary actuator, a servo valve, a valve controller, an encoder, diaphragm coupling, a magnetic powder brake, and auxiliary connections. One end of the output shaft of the actuator is equipped with the encoder, and the other end is connected to the brake through coupling. The encoder feeds back the angle signal to the valve controller, which processes the desired signal and feedback signal, and then outputs the control signal to the servo valve. The brake is used for loading, and the load torque can be set using its proprietary controller.

The setting of the experimental parameters is consistent with the nominal values presented in Table 1, and step response experiments were performed under the nine operating conditions. The rotation angle signal fed back by the encoder was written into the computer via an acquisition card, and the acquisition frequency was 1000 Hz. After filtering the data, step curves were obtained under all operating conditions, as shown in Figure 10(a). The rise time was regarded as the evaluation index of the system dynamic performance (i.e., the time when the initial value reaches 90% of the steady-state value), and the experimental results were compared with the calculation results of the theoretical model, as shown in Figure 10(b). The comparison results show that

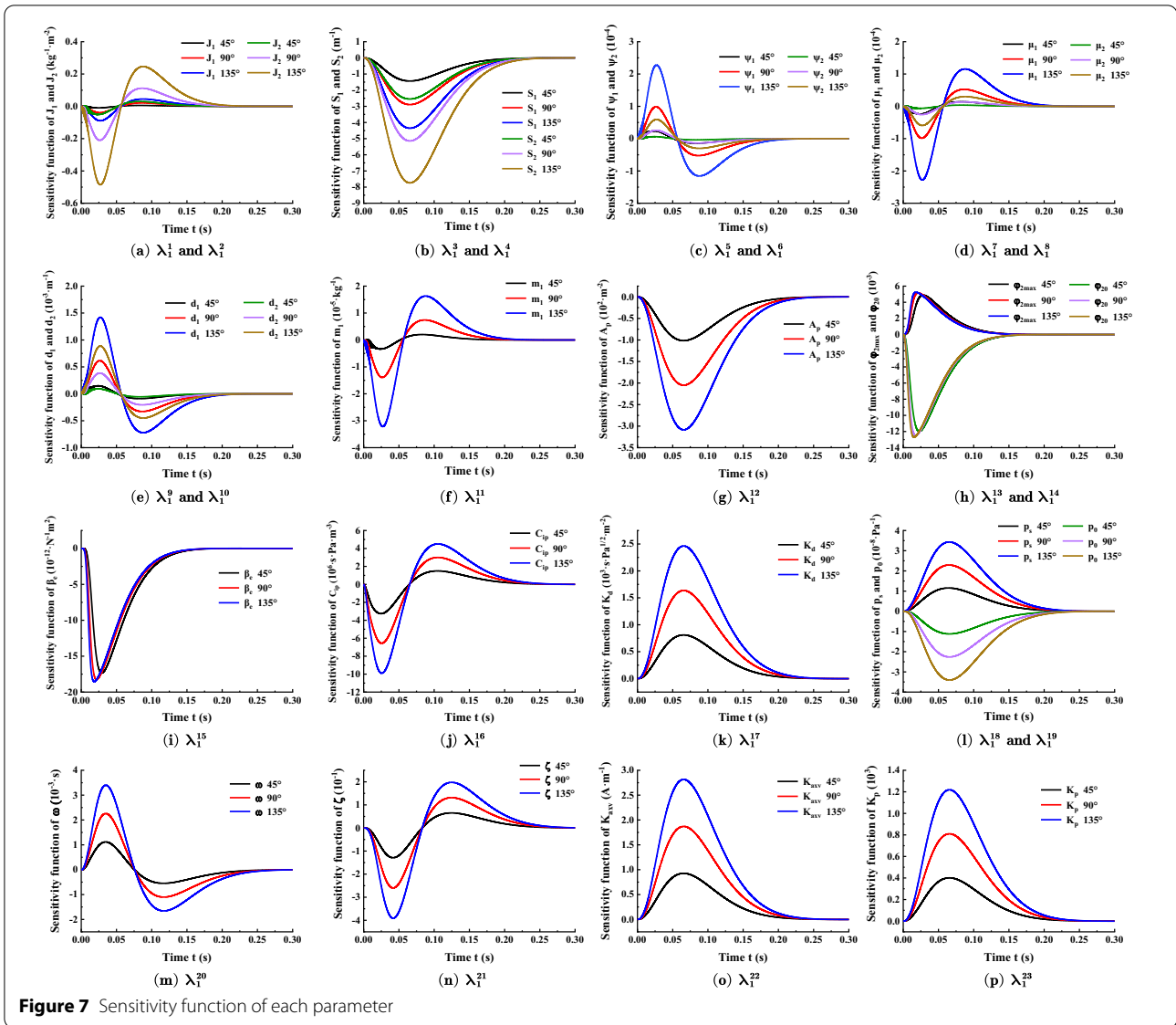


Figure 7 Sensitivity function of each parameter

under various operating conditions, the maximum error between the theoretical rise time and the experimental value did not exceed 7%, which verifies the accuracy of the system dynamics model established in this study.

4.2 Verification of Sensitivity Solution Results

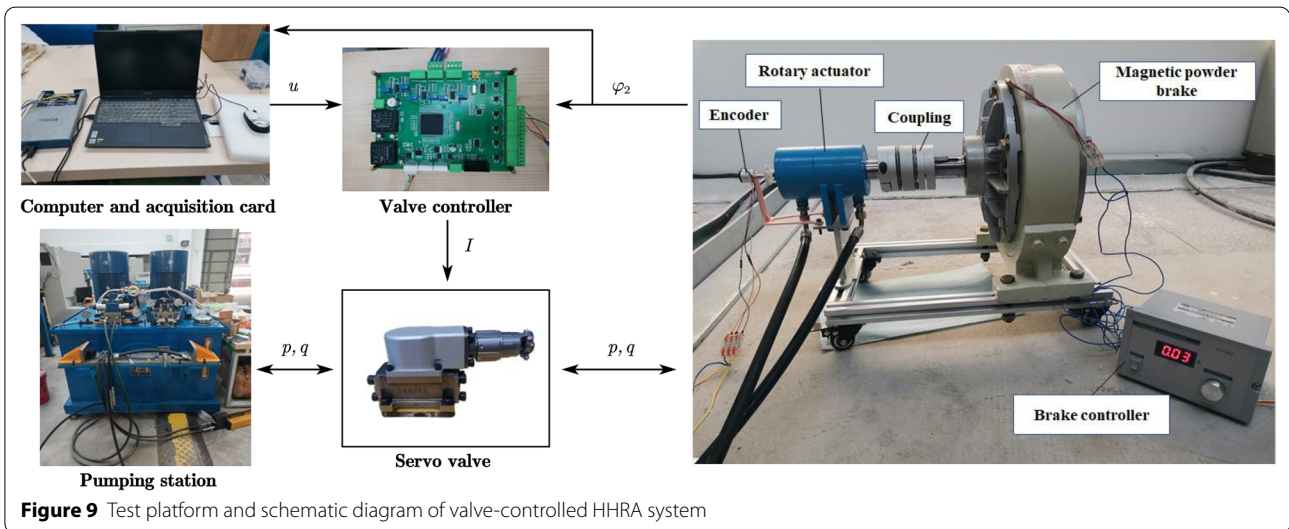
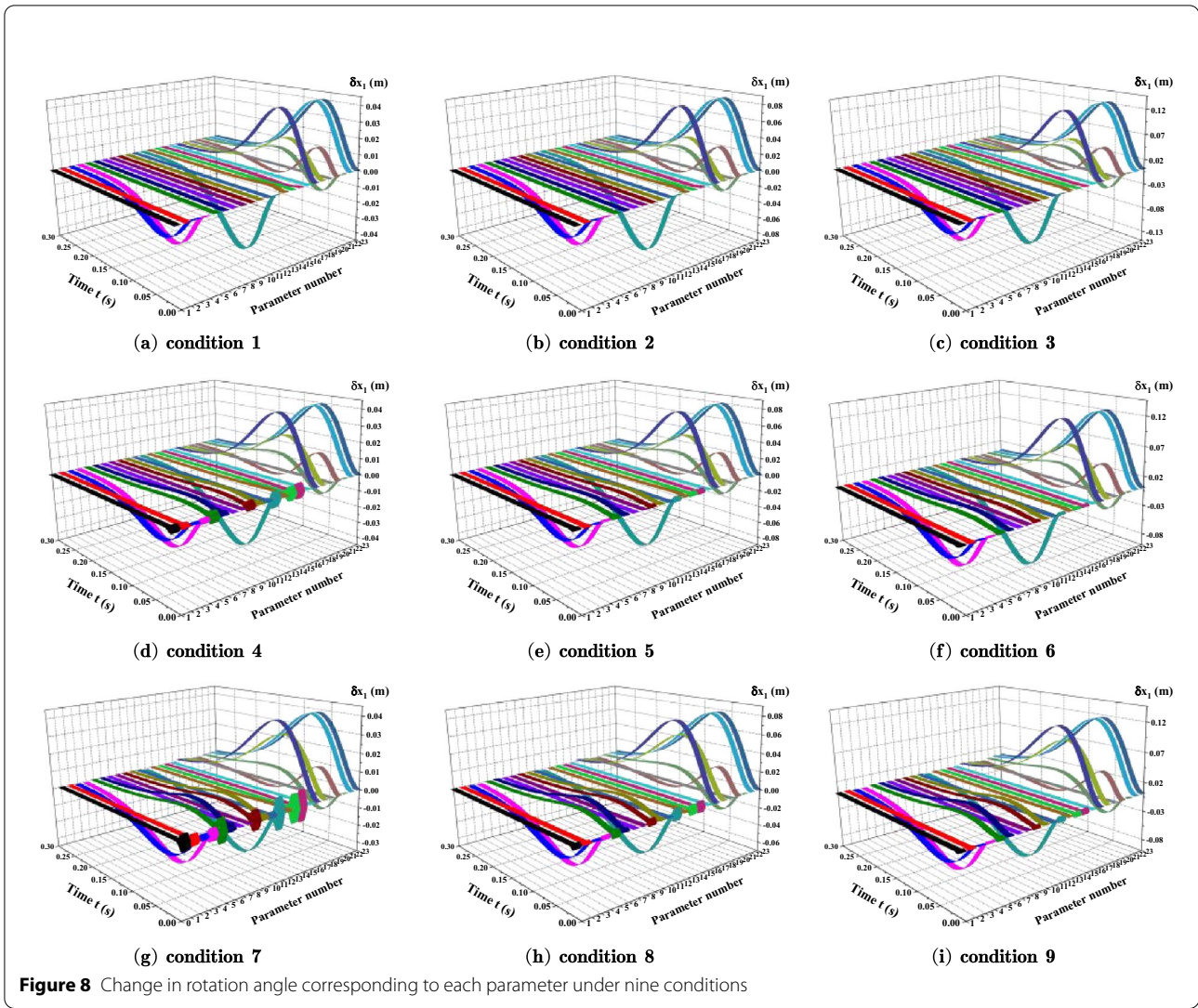
As mentioned above, the sensitivity solution was verified via co-simulation. First, the co-simulation model was established using MATLAB and Adams, and then four parameters showing rapid changes in the time scale were selected for sensitivity verification.

4.2.1 Co-Simulation Model

First, the 3D model was imported into Adams; subsequently, constraints and contacts were added. For the

moving components, a revolute joint was added to the output shaft, and a cylindrical joint was added to the piston. For other components, such as the housing and bearings, fixed pairs were added. Contacts were added between the piston and output shaft, as well as between the piston and housing. Hertz contact theory was used to calculate the contact force, and the corresponding contact parameters are listed in Table 3.

The plant was controlled using Adams. The hydraulic thrust F_{hyd} was used as the input signal of the system, and the output signals were the rotation angle and angular velocity of the output shaft. Finally, by combining Eqs. (13)–(18) and the Adams control plant, the co-simulation model for the valve-controlled HHRA system was established in MATLAB SIMULINK, as shown in Figure 11.



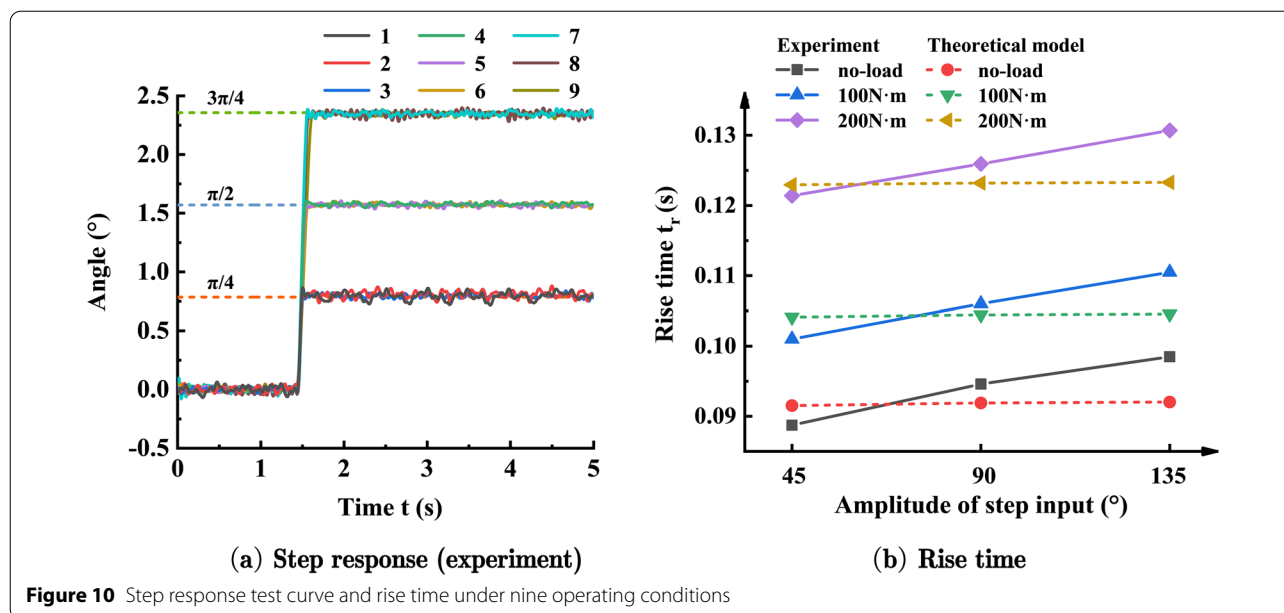


Figure 10 Step response test curve and rise time under nine operating conditions

Table 3 Setting of contact parameters

No.	Description	Value	Units
1	Stiffness	1×10^8	N/m
2	Force exponent	1.5	-
3	Damping	5×10^4	N·s/m
4	Penetration depth	1×10^{-4}	m
5	Dynamic coefficient	0.005	-

Next, the parameter sensitivity problem was solved using the co-simulation model and compared with the theoretical calculation results to complete the verification.

4.2.2 Verification of Parameter Sensitivity

To obtain the sensitivity solution from the co-simulation model, a certain parameter was changed by 10% while other parameters were maintained at the nominal value; subsequently, simulations were conducted to obtain the step response curve of the output shaft. By calculating the difference between the obtained curve and the curve prior to the parameter changes, the effect of the parameter change on the dynamic curve of the rotation angle was obtained and then compared with the results shown in Figure 8.

As mentioned in Section 3.2, parameters $\alpha_3, \alpha_4, \alpha_5, \alpha_6, \alpha_9, \alpha_{10}, \alpha_{12}, \alpha_{17}, \alpha_{18}, \alpha_{20}, \alpha_{21}, \alpha_{22},$ and α_{23} are more sensitive to the step response than the other parameters; therefore, these parameters should be prioritized. Parameters $\alpha_3, \alpha_4, \alpha_5, \alpha_6, \alpha_9, \alpha_{10},$ and α_{12} are the structural parameters of the actuator, which will not change in a short time under normal operating conditions, and the sensitivity curves of parameters α_{17}, α_{22} and α_{23} in Figure 8 are exactly the

same. Considering the parameters that change rapidly over time and for the convenience of expression, only parameters $\alpha_{18}, \alpha_{20}, \alpha_{21},$ and α_{23} were selected for verification. A comparison between the theoretical and co-simulation results is shown in Figures 12, 13, 14.

As shown by the curve, although the shapes of the theoretical and experimental curves are not completely consistent owing to the effects of the contact parameters, simulation step size, or other factors, the trend and range of the curves are similar for each parameter under different input conditions. This consistency proves the accuracy of the solution results of parameter sensitivity in the previous section and shows the effectiveness of using the first-order trajectory sensitivity analysis method to analyze the parameter sensitivity of the system. Because sensitivity analysis is used to evaluate the degree of influence of parameter variation on the system output, the slight error between the theoretical and experimental dynamic curves barely affects the analysis results. Therefore, the method proposed herein is applicable to the analysis of similar parameter sensitivity problems.

4.3 Analysis of Results

In this section, the sensitivity solution is analyzed more comprehensively. As shown in 8, the sensitivity function of each parameter changes with time. To quantify this dynamic process, a sensitivity index must first be determined. Farahat proposed four sensitivity indexes, among which the entirety index is reported to be the best index because it comprehensively considers all performance characteristics. In this study, the same index was used as the sensitivity index, and it is expressed as follows [21]:

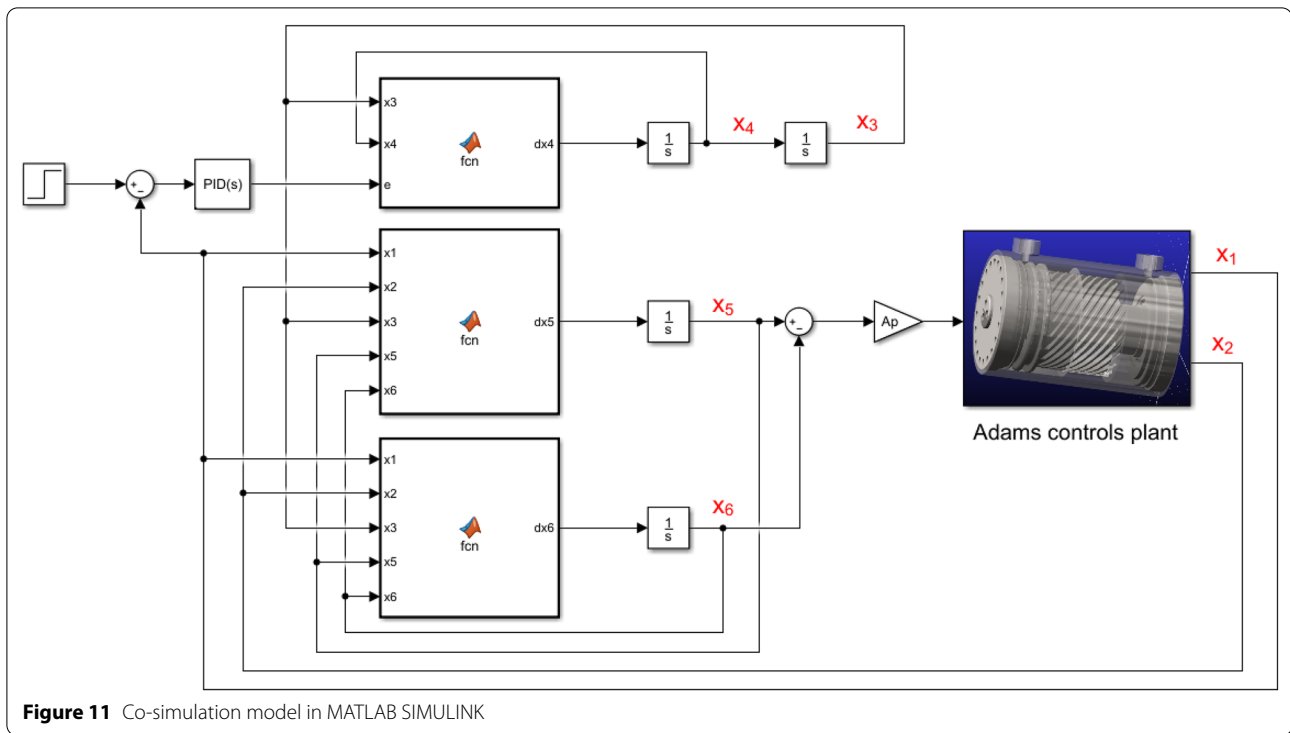


Figure 11 Co-simulation model in MATLAB SIMULINK

$$I_E = \int_0^T |\lambda'_i(t)| \delta\alpha_j dt. \tag{23}$$

Using Eq. (23), the curves in Figure 8 were integrated to obtain the sensitivity index values of the 23 parameters under nine operating conditions. The results are shown in Figures 15, 16, 17, where only parameters with a high sensitivity index are presented. Parameters whose sensitivity index is extremely low are omitted as their effects are negligible. The height of the column in the figure represents the integration of the absolute change in the output shaft rotation angle over the simulation time (0.3 s). Generally, the larger the height, the more sensitive is the output to the parameters.

As shown in Figures 15, 16, 17, when the system is under the same load conditions, the larger the step signal, the greater is the sensitivity index for a certain parameter. Moreover, the sensitivity index ranking of the parameters is the same when different step input signals are imposed. For the no-load condition, the order from high to low based on the sensitivity index of the parameters is as follows:

$$(I_E^0)\alpha_{12} = \alpha_{17} = \alpha_{22} = \alpha_{23} > \alpha_4 > \alpha_{18} > \alpha_3 > \alpha_{20} > \alpha_{21} > \alpha_{\text{others}}. \tag{24}$$

The corresponding quantitative relationship is expressed as

$$(I_E^0)\alpha_{12} = \alpha_{17} = \alpha_{22} = \alpha_{23} = 1.75\alpha_4 = 1.95\alpha_{18} = 2.33\alpha_3 = 3.06\alpha_{20} = 3.11\alpha_{21} > \alpha_{\text{others}}. \tag{25}$$

For the 100 N·m load condition,

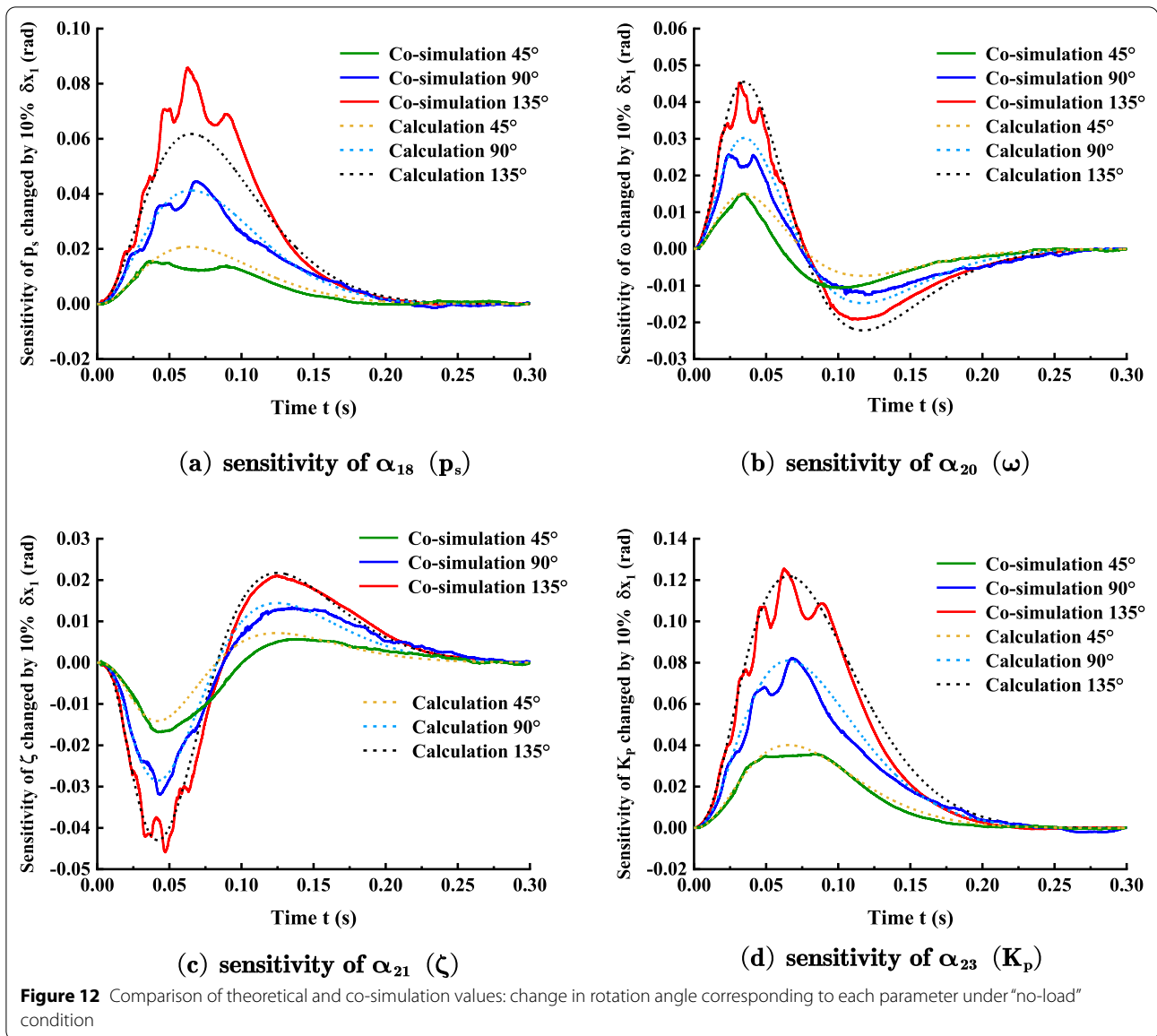
$$(I_E^{100})\alpha_{17} = \alpha_{22} = \alpha_{23} > \alpha_{12} > \alpha_{18} > \alpha_4 > \alpha_3 > \alpha_{20} > \alpha_{21} > \alpha_6 > \alpha_{10} > \alpha_5 > \alpha_9 > \alpha_{\text{others}}. \tag{26}$$

$$(I_E^{100})\alpha_{17} = \alpha_{22} = \alpha_{23} = 1.12\alpha_{12} = 1.62\alpha_{18} = 1.75\alpha_4 = 2.33\alpha_3 = 3.45\alpha_{20} = 3.5\alpha_{21} = 11.2\alpha_6 = 16.1\alpha_{10} = 17.5\alpha_5 = 21.2\alpha_9 > \alpha_{\text{others}}. \tag{27}$$

Meanwhile, for the 200 N·m load conditions,

$$(I_E^{200})\alpha_{17} = \alpha_{22} = \alpha_{23} > \alpha_{18} > \alpha_{12} > \alpha_4 > \alpha_3 > \alpha_{20} > \alpha_{21} > \alpha_6 > \alpha_{10} > \alpha_5 > \alpha_9 > \alpha_{\text{others}}. \tag{28}$$

$$(I_E^{200})\alpha_{17} = \alpha_{22} = \alpha_{23} = 1.28\alpha_{18} = 1.37\alpha_{12} = 1.75\alpha_4 = 2.33\alpha_3 = 4\alpha_{20} = 4.06\alpha_{21} = 4.42\alpha_6 = 6.39\alpha_{10} = 7\alpha_5 = 8.43\alpha_9 > \alpha_{\text{others}}. \tag{29}$$



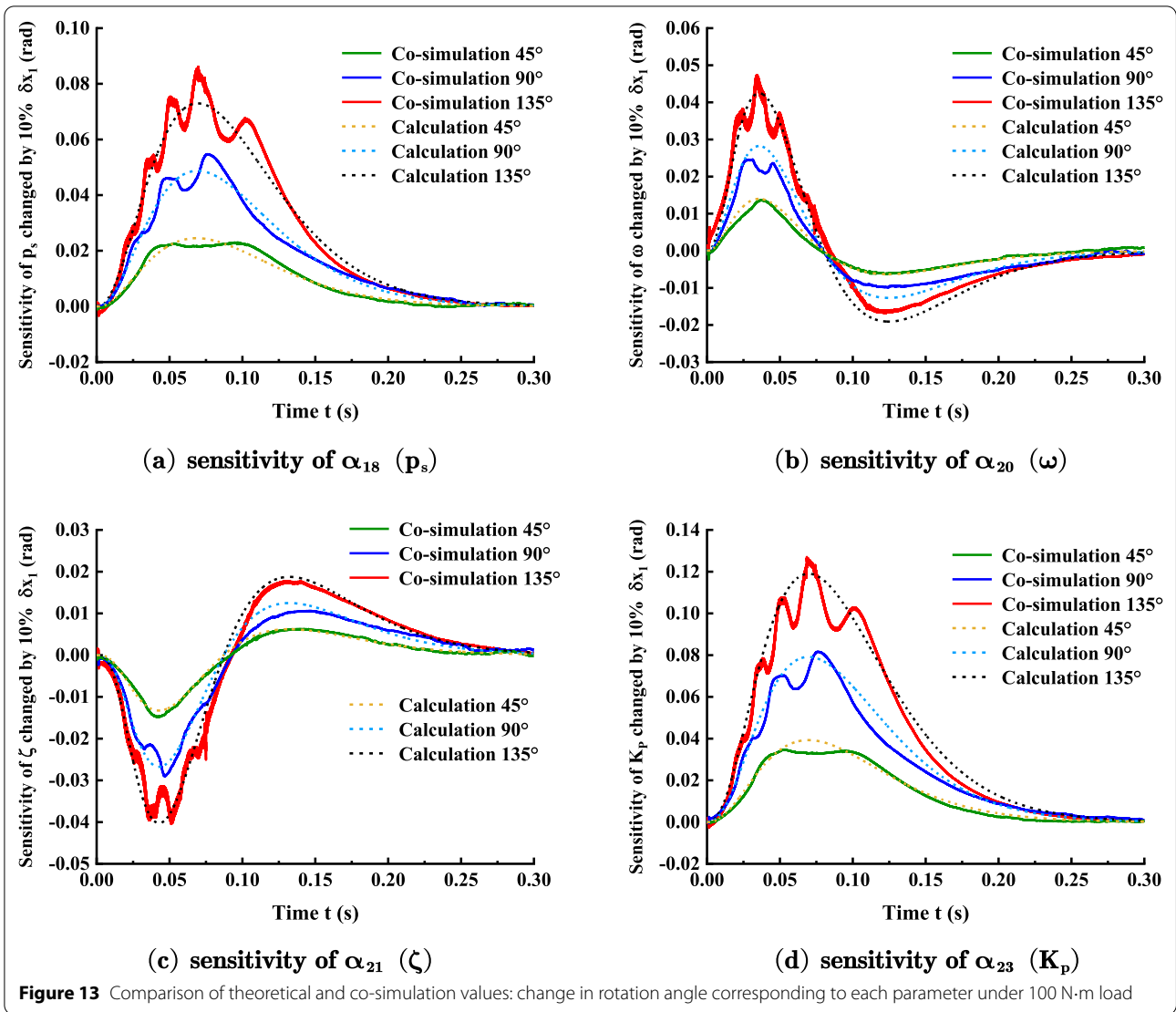
As indicated in Eqs. (24)–(29), when the system is under different load conditions, the sensitivity ranking of the parameters and the numerical relationship between the parameters change. To observe the changes in various parameters under different operating conditions, the sensitivity indices of the parameters under the nine operating conditions are summarized, as shown in Figure 18.

As shown in Figure 18, the sensitivity of each parameter increases with the step signal. However, as the system load increases, the sensitivity of some parameters (including S_1 , S_2 , Ψ_1 , Ψ_2 , d_1 , d_2 , K_d , p_s , K_{axv} , and K_p) increases, whereas the sensitivity of other parameters (including A_p , ω , and ζ) decreases. The sensitivity of the

former parameters increases significantly, whereas that the latter parameters decreases slightly. For parameters Ψ_1 , Ψ_2 , d_1 , and d_2 in particular, the order of magnitude of the sensitivity index is only 10^{-8} under the no-load condition; however, under a 200 N·m load, their sensitivity index values become tens of thousands of times that of the no-load condition.

5 Conclusions and Future Studies

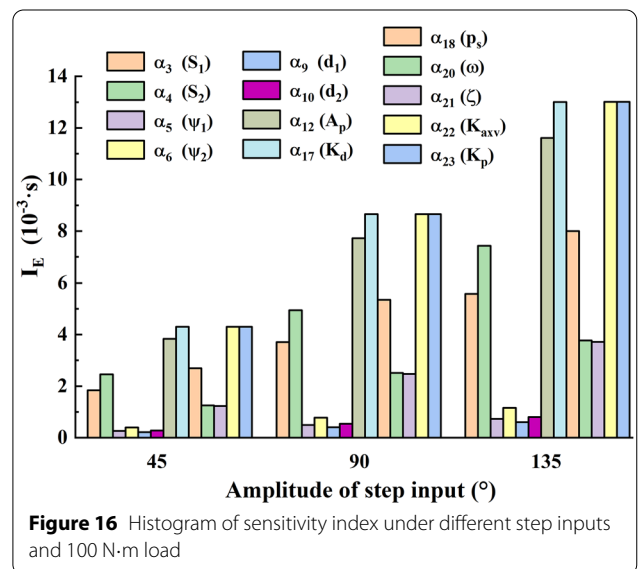
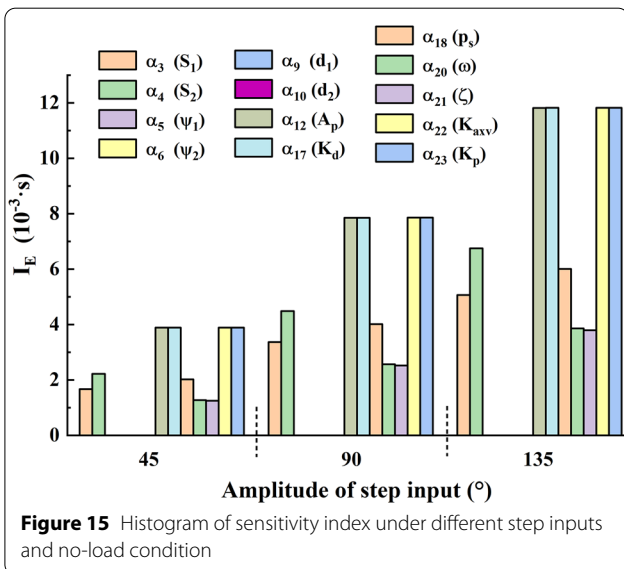
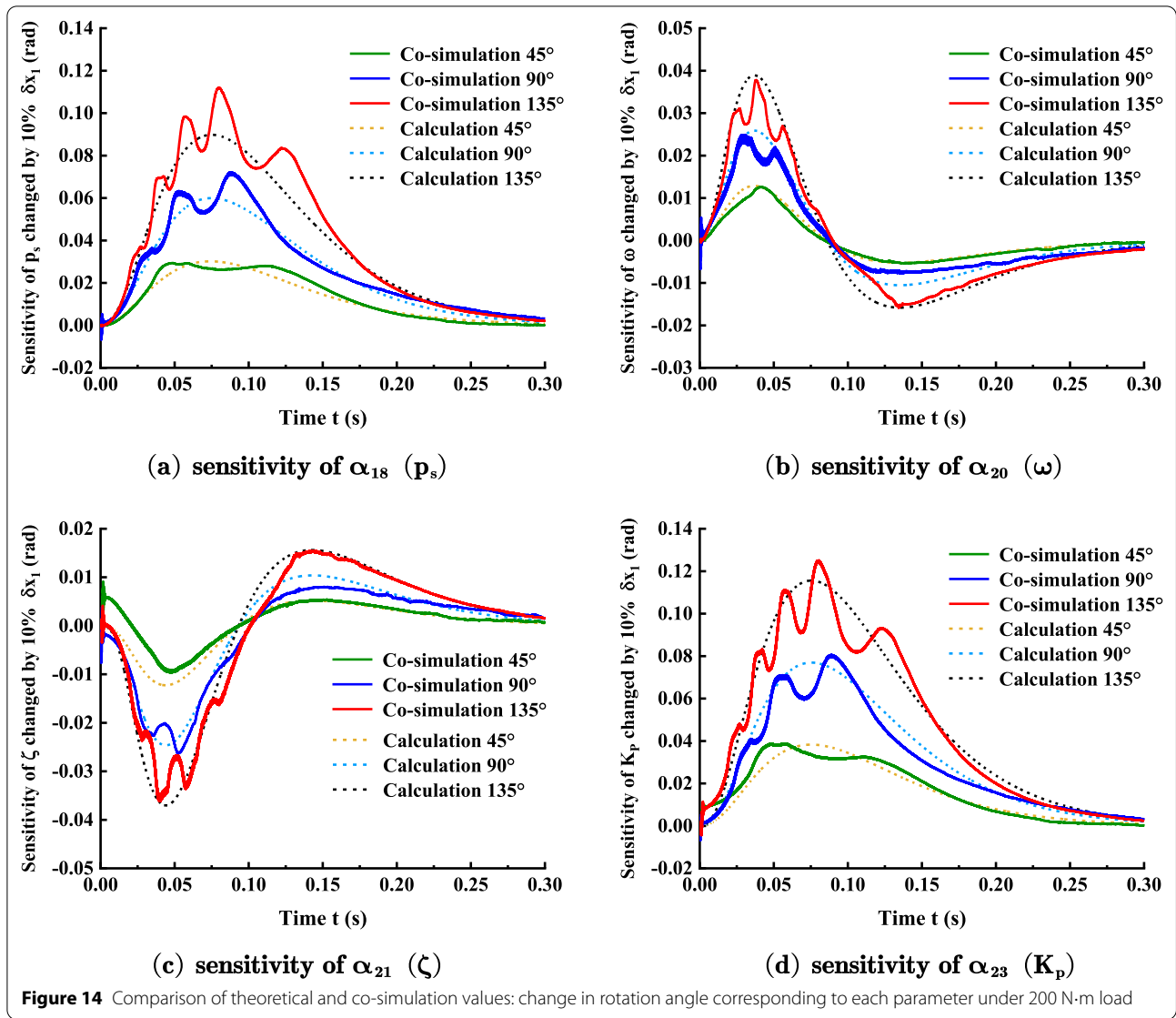
In this study, a complete mathematical model of a valve-controlled HHRA system with an angular displacement closed loop was established. Subsequently, the influence degree and law of 10% parameter change on the angular displacement step response were quantitatively

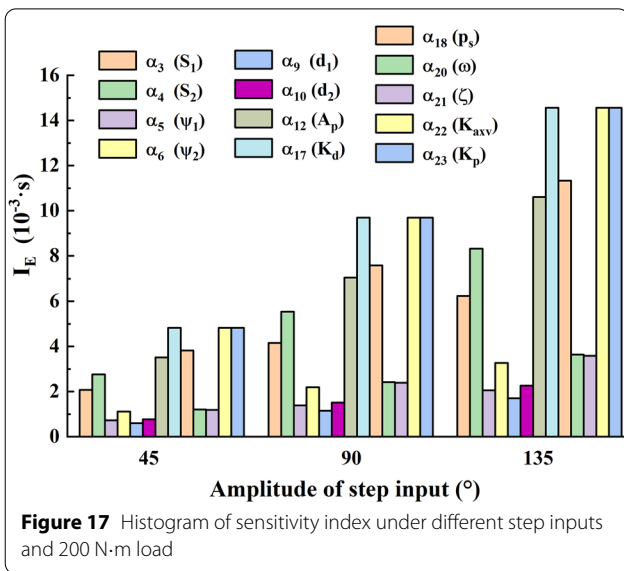


obtained using the first-order trajectory sensitivity analysis method. Finally, a prototype experiment and co-simulation were performed to verify the accuracy of the system dynamics model and sensitivity results, respectively. The good agreement between the theoretical and experimental (or co-simulation) values shows that the nonlinear system model established in this study can represent the dynamic characteristics of valve-controlled HHRA closed-loop systems effectively, and that the sensitivity equations are accurate. Therefore, the results of this study are reliable and can provide a basis for the

structural parameter optimization or control compensation of similar systems. The conclusions of the sensitivity analysis are as follows:

- (1) An analysis of the sensitivity of the angular displacement closed-loop system when the parameters changed by 10% showed that the sensitivity ranking and values of the parameters were different under different operating conditions. In general, under the nine operating conditions involving different step inputs and loads described herein, the perturbation



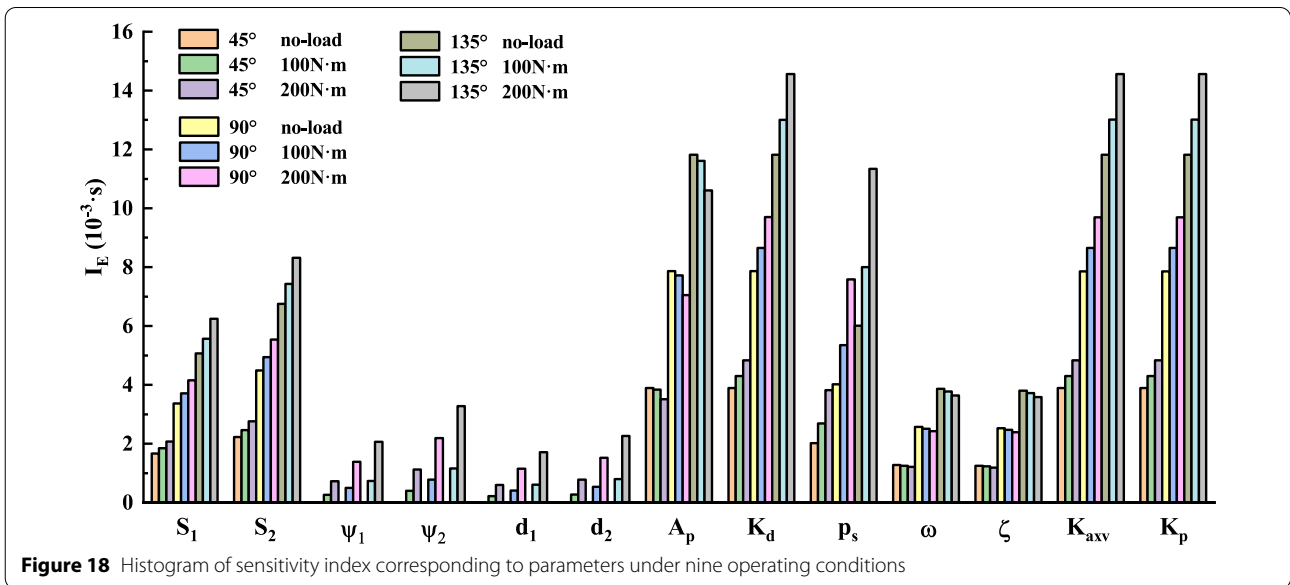


of structural parameters S_1 , S_2 , Ψ_1 , Ψ_2 , d_1 , d_2 , and A_p of the HHRA, operating parameters K_d and p_s , servo valve parameters ω , ζ , and K_{axv} , and the control parameter K_p significantly affected the dynamic characteristics of the system. Moreover, the sensitivity of these parameters increased significantly with an increase in the step input signal. For the

other parameters, the effect of small-scale perturbations was negligible.

- (2) For structural parameters with high sensitivity, sensitivity can be reduced by selecting the appropriate parameters or optimizing the structure. For operating parameters with high sensitivity and rapid perturbation, their fluctuations must be reduced when designing the system. The parameters of the servo valve are highly sensitive; therefore, the values of the valve parameters used during modeling should be the same as those of the actual system because an incorrect value may cause significant deviation between the actual situation and design requirements. The control parameters are expected to significantly affect the system output because the dynamic characteristics of the system are often altered when the controller parameters are adjusted.

In future studies, the valve-controlled HHRA system designed in this study will be used to operate legged robots because the characteristics of helical hydraulic cylinders are suitable for high-speed robots, which require a compact structure and a high explosive force. In addition, to adapt the designed system to systems with different control performance requirements, a sensitivity analysis of the parameters of the system will be performed using different control algorithms.



Acknowledgements

The authors sincerely thank the engineers in Xiangyang Hangyu Electro-mechanical Hydraulic Application Technology Co. Ltd. for their assistance in processing and experimentation.

Author Contributions

JZ and BX were responsible for the entire trial; KZ was a major contributor in writing the manuscript; MG, HZ, XW, HH, QS assisted in procurement, experiment, etc. All authors have read and approved the final manuscript.

Authors' Information

Kun Zhang, born in 1996, is currently a Ph.D. candidate at *State Key Laboratory of Fluid Power and Mechatronic Systems, Zhejiang University, China*. His research interests include hydraulic systems and robotic control.

Junhui Zhang, born in 1983, is currently deputy director at *State Key Laboratory of Fluid Power and Mechatronic Systems, Zhejiang University, China*. He received his Ph.D. degree from *Zhejiang University, China*, in 2012. His research interests include hydraulic transmissions, hydraulic components, and hydraulic robots.

Minyao Gan, born in 1978, is currently an engineer at *Shanghai Marine Equipment Research Institute, China*.

Huaizhi Zong, born in 1995, is currently a Ph.D. candidate at *State Key Laboratory of Fluid Power and Mechatronic Systems, Zhejiang University, China*. His research interests include hydraulic components and robotic design.

Ximeng Wang, born in 1997, is currently a master candidate at *State Key Laboratory of Fluid Power and Mechatronic Systems, Zhejiang University, China*. His research interests include electric control systems and robotic control.

Hsinpu Huang, born in 1995, is currently a master candidate at *State Key Laboratory of Fluid Power and Mechatronic Systems, Zhejiang University, China*. His main research interests include additive manufacturing and robotic design.

Qi Su, born in 1987, is currently an assistant research fellow at *State Key Laboratory of Fluid Power and Mechatronic Systems, Zhejiang University, China*. He received his Ph.D. degree from *Zhejiang University, China*, in 2016. His primary research interests include electromechanical systems and hydraulic valves.

Bing Xu, born in 1971, is a professor at *Zhejiang University, China*. He served as a director at *State Key Laboratory of Fluid Power and Mechatronic Systems, Zhejiang University, China*. His main research interests include hydraulic components and systems.

Funding

Supported by National Natural Science Foundation of China (Grant No. 51922093), Scientific Research Fund of Zhejiang Provincial Education Department of China (Grant No. Y202148352), and Major Science and Technology Projects in Ningbo of China (Grant No. 2019B10054).

Competing Interests

The authors declare no competing financial interests.

Author Details

¹State Key Laboratory of Fluid Power and Mechatronic Systems, Zhejiang University, Hangzhou 310027, China. ²Shanghai Marine Equipment Research Institute, Shanghai 200031, China.

Received: 11 December 2021 Revised: 26 March 2022 Accepted: 22 April 2022

Published online: 08 June 2022

References

- N M Tri, D X Ba, K K Ahn. A gain-adaptive intelligent nonlinear control for an electrohydraulic rotary actuator. *International Journal of Precision Engineering and Manufacturing*, 2018, 19(5): 665-673.
- S B Li. *Dynamic characteristics study of helical oscillating hydraulic actuator*. Changsha: Central South University, 2012. (in Chinese)
- C Z Wang. *Research on technology of hydraulic individual blade pitch control for horizontal axis marine current turbine*. Hangzhou: Zhejiang University, 2018. (in Chinese)
- G J Wang, X C Liang. A new type of screw rotary actuator of robot, *IEEE International Conference on Robotics and Biomimetics*, 2004: 495-498.
- R G Shen. *High pressure swing hydraulic actuator structure and efficiency research based on the principle of the double helix rotation*. Hangzhou: Zhejiang University, 2013. (in Chinese)
- Parker. Helac Products | Parker Cylinder Division. <https://promo.parker.com/promotionsite/helac/us/en/products>. Accessed November 29, 2021.
- Hengli. Mobile machinery cylinders-aerial work platform cylinder. <https://www.hengliamerica.com/product/Mobile-Machinery-Cylinders/Aerial-Work-Platform-Cylinder>. Accessed 29 Nov 2021.
- HKS. HKS – Products. <https://www.hks-partner.com/en/products>. Accessed 29 Nov 2021.
- ECKART. All products / Eckart GmbH. <https://www.eckart-hydraulics.com/en/products/all-products.html>. Accessed 29 Nov 2021.
- P P Weyer. Rotary Actuator: US, 4373426A. 1983-02-15.
- D R Weyer. Rotary Actuator: EP, 0825350A1. 1998-02-25.
- J C Shu. Helical Rotary Actuator: US, 20120079901A1. 2012-04-05.
- Y Yang, X Guo, S D Yang, et al. Strength optimization design of a helical hydraulic rotary actuator. *Advanced Materials Research, Trans Tech Publications Ltd*, 2012, 544: 139-144.
- S B Li, Y L Liu, J Q Li. Transmission efficiency analysis and experiment research on helical oscillating hydraulic actuator. *Applied Mechanics and Materials, Trans Tech Publications Ltd*, 2014, 511: 623-627.
- Y P Shi, Y Zang. Efficiency analysis and improving method of the screw rotary actuator. *Chinese Hydraulics & Pneumatics*, 2011, 5: 84-86. (in Chinese)
- J Liu. *Spiral swing hydraulic actuator analysis and simulation research*. Wuhan: Wuhan University of Technology, 2014. (in Chinese)
- T Boaventura, J Buchli, C Semini, et al. Model-based hydraulic impedance control for dynamic robots. *IEEE Transactions on Robotics*, 2015, 31(6): 1324-1336.
- D M Hamby. A review of techniques for parameter sensitivity analysis of environmental models. *Environmental Monitoring and Assessment*, 1994, 32(2): 135-154.
- M F A Rahmat, A R Husain, K Ishaque, et al. Modeling and controller design of an industrial hydraulic actuator system in the presence of friction and internal leakage. *International Journal of Physical Sciences*, 2011, 6(14): 3502-3517.
- M J Vilenius. The application of sensitivity analysis to electrohydraulic position control servos. *Journal of Dynamic Systems, Measurements and Control*, 1983, 105: 77-82.
- S Farahat, H Ajam. Sensitivity analysis of parameter changes in nonlinear hydraulic control systems. *International Journal of Engineering*, 2005, 18(3): 239-252.
- E Parente Jr, J B M de Sousa Jr. Design sensitivity analysis of nonlinear structures subjected to thermal loads. *Computers & Structures*, 2008, 86(11-12): 1369-1384.
- J W Hall, S A Boyce, Y Wang, et al. Sensitivity analysis for hydraulic models. *Journal of Hydraulic Engineering*, 2009, 135(11): 959-969.
- M M Kamiński. Structural sensitivity analysis in nonlinear and transient problems using the local response function technique. *Structural and Multidisciplinary Optimization*, 2011, 43(2): 261-274.
- S D Kim, H S Cho, C O Lee. A parameter sensitivity analysis for the dynamic model of a variable displacement axial piston pump. *Proceedings of the Institution of Mechanical Engineers, Part C: Journal of Mechanical Engineering Science*, 1987, 201(4): 235-243.
- M T Pietola, M J Vilenius. Theoretical and experimental study of the effect of varying load on the dynamics of a P, MRC or P+ PID/x controlled electrohydraulic position servo system. *Proceedings of the Institution of Mechanical Engineers, Part C: Mechanical Engineering Science*, 1989, 203(4): 267-274.
- M T Pietola, M J Vilenius. Sensitivity of a position servo system to variations in the constructive parameters in transient and steady state. *Mechanism and Machine Theory*, 1991, 26(3): 261-274.
- X D Kong, B Yu, L X Quan, et al. Nonlinear mathematical modeling and sensitivity analysis of hydraulic drive unit. *Chinese Journal of Mechanical Engineering*, 2015, 28(5): 999-1011.
- X D Kong, K X Ba, B Yu, et al. Trajectory sensitivity analysis of first order and second order on position control system of highly integrated valve-controlled actuator. *Journal of Mechanical Science and Technology*, 2015, 29(10): 4445-4464.

- [30] K X Ba, B Yu, Z J Gao, et al. Parameters sensitivity analysis of position-based impedance control for bionic legged robots' HDU. *Applied Sciences*, 2017, 7(10): 1035.
- [31] K X Ba, B Yu, X D Kong, et al. Parameters sensitivity characteristics of highly integrated valve-controlled actuator force control system. *Chinese Journal of Mechanical Engineering*, 2018, 31:43
- [32] K X Ba, B Yu, Q X Zhu, et al. Second order matrix sensitivity analysis of force-based impedance control for leg hydraulic drive system. *Robotics and Autonomous Systems*, 2019, 121: 103265.
- [33] J Huang, H L An, L Lang, et al. A data-driven multi-scale online joint estimation of states and parameters for electro-hydraulic actuator in legged robot. *IEEE Access*, 2020, 8: 36885-36902.

Submit your manuscript to a SpringerOpen[®] journal and benefit from:

- ▶ Convenient online submission
- ▶ Rigorous peer review
- ▶ Open access: articles freely available online
- ▶ High visibility within the field
- ▶ Retaining the copyright to your article

Submit your next manuscript at ▶ [springeropen.com](https://www.springeropen.com)
